Chapter 10
New Na^+ Superionic Conductor Narpsio Glass-Ceramics

Toshinori Okura and Kimihiro Yamashita

Abstract This review article describes a series of studies on glass-ceramic Na^+ superionic conductors with the $Na_5YSi_4O_{12}$ (N5)-type structure and with a $Na_{3+3x-y}R_{1-x}P_ySi_{3-y}O_9$ composition, where R is a rare earth element. In the crystallization of N5-type glass-ceramics, its relatives ($Na_3YSi_3O_9$ (N3)- and $Na_9YSi_6O_{18}$ (N9)-type glass-ceramics) structurally belonging to the family of $Na_{24-3x}Y_xSi_{12}O_{36}$ were found to crystallize as the precursor phase at low temperatures. In order to produce N5 single-phase glass-ceramics, the concentration of both phosphorus and rare earth was found important. The meaning of the composition was evaluated by kinetic study on the phase transformation of metastable N3 or N9 phases to stable N5 phase with Na^+ superionic conductivity. The possible combinations of x and y became more limited for the crystallization of the superionic conducting phase as the ionic radius of R increased, while the Na^+ conduction properties were more enhanced in the glass-ceramics of larger R. These results are discussed in view of the structure and the conduction mechanism. Also discussed were the microstructural effects on the conduction properties, which were dependent upon the heating conditions of crystallization. These effects were understood in relation to the grain boundary conduction properties as well as the transmission electron microstructural morphology of grain boundaries. Recent research into the effects of microstructure on conduction properties and microstructural control of Na^+ superionic conducting glass-ceramics is also introduced. The optimum conditions for crystallization are discussed with reference to the conduction properties and the preparation of crack-free N5-type glass-ceramics. The effects of substituting Si with other elements exhibiting tetrahedral oxygen coordination and substituting Y with various rare earth elements are also

T. Okura (✉)
Department of Applied Chemistry, School of Advanced Engineering, Kogakuin University, Tokyo, Japan
e-mail: okura@cc.kogakuin.ac.jp

K. Yamashita
Institute of Biomaterials and Bioengineering, Tokyo Medical and Dental University, Tokyo, Japan
e-mail: yama-bcr@tmd.ac.jp

T. Onishi (ed.), *Theoretical Chemistry for Advanced Nanomaterials*,
https://doi.org/10.1007/978-981-15-0006-0_10

discussed in the context of the ionic conductivity of these N5-type glass-ceramics. In addition, results on the improvement in superconductivity by Na^+ ion implantation and control of the structure by bias crystallization of glasses in an electric field are presented.

Keywords Superionic conductor · Glass-ceramics · Crystallization · Microstructure · Ion implantation · Bias crystallization

10.1 Introduction

The use of glass-making processing is favorablefor the fabrication of Na^+ conducting electrolyte tubes, which has been the key to the technological development of 1 MW Na/S secondary battery plants. However, the processing technique cannot be applied to well-known β- and β″-aluminas (e.g., $NaAl_{11}O_{17}$ and $NaAl_5O_8$) and Nasicons ($Na_{1+x}Zr_2P_{3-x}Si_xO_{12}$) because their high inclusion of Al_2O_3 or ZrO_2 brings about the inhomogeneous melting or crystallization of glasses. Alternatively, Nasicon-like glass-ceramics were synthesized using a composition with lower content of ZrO_2 ($mNa_2O{\cdot}xZrO_2{\cdot}yP_2O_5{\cdot}(100{-}m{-}x{-}y)SiO_2$ [m = 20, 30 mol %]). However, the conductivities (σ) attained were, at most, as high as $\sigma_{300} = 2 \times 10^{-2}$ S/cm at 300 °C with the activation energies (E_a) of ca. 30 kJ/mol [1]. These low conductivities were attributed to the crystallization of the poorly conductive rhombohedral phase in these Nasicon-like materials [1]. $Na_5YSi_4O_{12}$ (N5), which comprises 12-$(SiO_4)^{4-}$-tetrahedra-membered skeleton structure (Fig. 10.1) [2, 3], is another Na^+ superionic conductor with $\sigma_{300} = 1 \times 10^{-1}$ S/cm and $E_a = 25$ kJ/mol [4–7]. A pioneering work on N5-type glass-ceramics was performed by Banks et

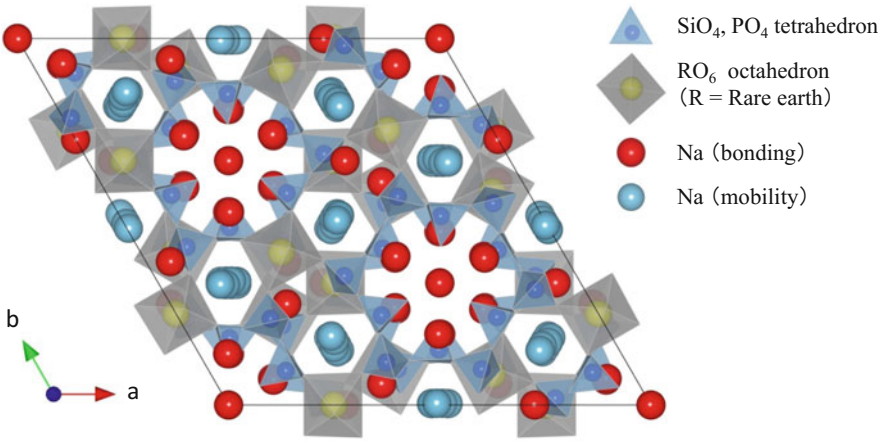

Fig. 10.1 Crystal structure of $Na_5YSi_4O_{12}$ [4]. Reprinted from Solid State Ionics 285 (2016) 143, Copyright 2016, with permission from Elsevier

al. on the family of N5-type materials by substituting Y with Er, Gd, or Sm [8]. However, their results were not completely satisfactory because of the relatively lower conductivities of $\sigma_{300} < 2 \times 10^{-2}$ S/cm than the reported values of N5 [8]. This discrepancy may possibly have arisen from the occurrence of a less conductive metastable phase during crystallization [9], as discussed below.

Contrary to the results of Banks et al., we obtained glass-ceramics where $\sigma_{300} = 1 \times 10^{-1}$ S/cm and $E_a = 20$ kJ/mol [10]; these compounds were based on the phosphorus-containing N5-type materials discovered in the Na_2O-Y_2O_3-P_2O_5-SiO_2 system [10]. These N5-type materials, in addition to $Na_3YSi_3O_9$ (N3)-type materials [11–13], were obtained with the composition formula originally derived for N3-type solid solutions and expressed as follows [14]:

$$Na_{3+3x-y}Y_{1-x}P_ySi_{3-y}O_9 \ (x < 0.6, \quad y < 0.5) \tag{10.1}$$

With the aim of searching for more conductive glass-ceramic N5-type materials, the verification of the validity of the general composition

$$Na_{3+3x-y}R_{1-x}P_ySi_{3-y}O_9 \ (R = \text{a rare earth element}) \tag{10.2}$$

for the synthesis of other types of rare earth N5-type glass-ceramics was studied first. Formula 2 is rewritten with formula 3 according to the formula N5.

$$Na_{4(3+3x-y)/3}Y_{4(1-x)/3}P_{4y/3}Si_{4(3-y)/3}O_{12} \tag{10.3}$$

In relation to previous works [10, 14], formula 2 was employed in this work, and formula 3 is referred to in the results. The trivalent ions employed here for R^{3+} were Sc^{3+}, In^{3+}, Er^{3+}, Gd^{3+}, Sm^{3+}, Eu^{3+}, Nd^{3+}, La^{3+}, and Y^{3+}. These results are to be interpreted in terms of the effect of the rare earth ions on the crystallization of the N5-type phase in glasses [15–20].

Interestingly, in the course of the fundamental studies on the glass-ceramics $Na_{3+3x-y}R_{1-x}P_ySi_{3-y}O_9$, we have found the crystallization of those N3- and $Na_9YSi_6O_{18}$ (N9)-type phases as the precursors in the glasses [21]. These are the analogues to the silicates N3 and N9 [10, 22] and therefore are the same members of the family of $Na_{24-3x}Y_xSi_{12}O_{36}$ [12] as N5. Although we had also successfully synthesized those materials by the solid-state reactions of powders with the above composition of various sets of the parameters x and y [10, 22], the metastability of those precursor phases had not been noticed in the synthesis. It has been observed that such precursor phases were transformed to the Na^+ superionic conducting phase on specimens with appropriate sets of x and y. The present review paper deals with the thermodynamic and kinetic studies on the phase transformation of metastable phases to the stable phase with Na^+ superionic conductivity. The superiority of our present materials to the other silicate N5 will also be detailed based on the kinetic results.

The microstructure of a glass-ceramics, including neck growth among grains as well as grain size, is generally affected by the crystallization process [23]. As

the abovementioned devices utilize the dc conduction properties of Na^+ superionic conductors, another aim was to study the microstructural effects on the conduction properties of a whole glass-ceramic [24–28]. Special attention was paid to the analysis of grain boundary properties using the Na_2O-Y_2O_3-P_2O_5-SiO_2 system. For the analysis of grain boundary properties, as discussed below, composition dependences on the conductivity of sodium silicophosphate glasses containing Y_2O_3 were also introduced in the Na_2O-Y_2O_3-P_2O_5-SiO_2 system. For convenience, the present materials are abbreviated as Narpsio, taken from the initials of the Na_2O-R_2O_3-P_2O_5-SiO_2 system.

10.2 Materials

10.2.1 Glasses and Glass-Ceramics

We successfully produced the Narpsio family by the following methods: (i) solid-state reactions of powders [10, 22], (ii) sol-gel method [19, 29], and (iii) crystallization of glasses [30]. In considering practical applications such as Na/S batteries, the present Narpsio materials may be expected to show advantages over the aluminas, both in lowering the heat treatment temperatures and in fabricating various shapes because of the ease of glass-making. The latter point closely depends on the glass-ceramic processing technology.

Precursor glasses were prepared from reagent-grade oxides of anhydrous Na_2CO_3, R_2O_3 (R = Y, Sc, In, Er, Gd, Sm, Eu, Nd, La), $NH_4H_2PO_4$, and SiO_2; the mechanically mixed powders according to formula 2 or appropriate compositions shown below were melted at 1350 °C for 1 h after calcination at 900 °C for 1 h. The melts were quickly poured into a graphite cylinder and then annealed at 500 °C for 3 h, giving Narpsio glasses. The composition parameters studied were in the range of $0.2 < x < 0.6$ and $0 < y < 0.5$ of formula 2. As shown below, grain boundary conduction properties are discussed in relation to the properties of glasses. For the evaluation of the composition dependence of conductivity in Na^+ conducting glasses, various sodium-yttrium silicophosphate glass specimens with different atomic ratios of Na/(P+Si) and Na/Y were also prepared.

Crystallization was carried out according to a previous report [14]; bulk glasses were heated at a rate of 75 °C/h to a temperature approximately 50 °C above the glass transition point, which had been determined in advance by differential thermal analysis (DTA). This pretreatment was performed in order to obtain homogeneous nucleation [23]. After annealing for 1 h, the specimens were heated at temperatures of 800–1100 °C, depending on the composition, for 0.5 to 72 h, and thereafter slowly cooled in a furnace with a decreasing rate of 150 °C/h to room temperature. These quenched glasses or glass-ceramic specimens were polished with 0.5 μm diamond paste and thereafter subjected to conductivity measurements.

For the description of a specific Narpsio, *R* of the term will be replaced, respectively, with Y, Sc, In, Er, Gd, Sm, Eu, Nd, and La as Y-Narpsio, Sc-Narpsio, In-Narpsio, Er-Narpsio, Gd-Narpsio, Sm-Narpsio, Eu-Narpsio, Nd-Narpsio, and La-Narpsio for Y_2O_3, Sc_2O_3, In_2O_3, Er_2O_3, Gd_2O_3, Sm_2O_3, Eu_2O_3, Nd_2O_3, and La_2O_3, respectively.

10.2.2 Characterization

10.2.2.1 AC Impedance Measurement

Ionic conductivities were evaluated by the complexim pedance method on cylindrical glasses or glass-ceramics, typically 15 mm in diameter and 2 mm in thickness. Electrodes were prepared by sputtering of gold on polished surfaces. The applied ac field ranged from 5 to 10 MHz in frequency. The temperature dependence of the conductivity was measured similarly at several temperatures ranging from room temperature to 350 °C. The complex impedance or admittance loci of glass and glass-ceramics were analyzed by an equivalent circuit (Fig. 10.2), which was experimentally found to comprise one and two semicircles in Narpsio glasses and glass-ceramics, respectively. The two intercepting points on the real axis are interpreted as the resistance of the crystallized grains ($R_{G(c)}$) and the total resistance

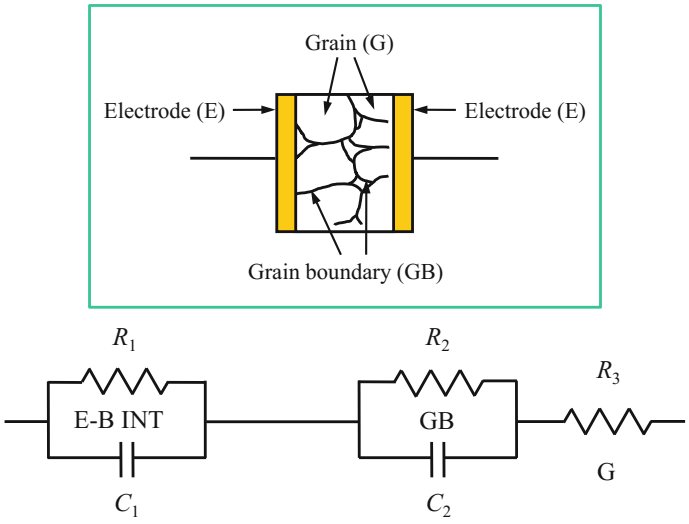

Fig. 10.2 Equivalent circuit employed for the admittance analysis. E-B INT, GB, and G represent the electrode-bulk interface, grain boundaries, and grains, respectively, and (R_1, C_1), (R_2, C_2), and R_3 are their resistances and capacitances [30]. Reprinted by permission from Springer Nature: Springer J. Electroceram. 24 (2010) 83, COPYRIGHT (2010)

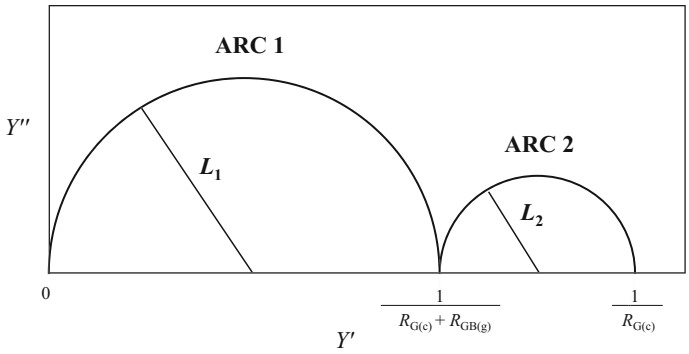

Fig. 10.3 Idealized diagram of complex admittance for glass-ceramics, in which arc 1 (ARC 1) and arc 2 (ARC 2) are related to the crystallized grains (G(c)) and remaining glasses (GB(g)). L_1, L_2, $R_{G(c)}$, and $R_{GB(g)}$ are, respectively, the radii of arcs 1 and 2 and the resistances of G(c) and GB(g) [30]. Reprinted by permission from Springer Nature: Springer J. Electroceram. 24 (2010) 83, COPYRIGHT (2010)

of the grains and remaining glassy grain boundaries ($R_{GB(g)}$). Assume the complex admittance diagram shown in Fig. 10.3, where the parameters L_1 and L_2 are set here as the radii of the two arcs 1 and 2. Those parameters are related to one another as follows:

$$L_1 \propto 1/\left(R_{G(c)} + R_{GB(g)}\right) \tag{10.4}$$

and

$$L_2 \propto \left(1/R_{G(c)}\right) - 1/\left(R_{G(c)} + R_{GB(g)}\right) \tag{10.5}$$

Then,

$$L_2/L_1 = R_{GB(g)}/R_{G(c)} \tag{10.6}$$

Therefore, in an ideal glass-ceramic where residual glass would have negligible influence on the total, arc 2 would be much smaller than arc 1, because $L_2/L_1 \rightarrow 0$.

10.2.2.2 X-Ray Diffraction

The form of the powder X-ray diffraction (XRD) data obtained from a material will depend upon the crystal structure it adopts. This structure is delineated by the lattice type, crystal class, unit cell parameters, and the distribution of the various ion and molecule types within the unit cell. The number and positions, in terms of 2θ, of the reflections depend upon the cell parameters, crystal class, lattice type, and

wavelength used to collect the data, while peak intensity depends upon the types of atoms present and their positions.

As a result of the enormous range of different structures which materials adopt, nearly all crystalline solids have a unique powder X-ray diffraction pattern in terms of the positions of the observed reflections and the peak intensities. In mixtures of compounds, each crystalline phase present will contribute to the powder diffraction pattern in its own unique set of lines. The relative intensity of line sets from mixtures will depend on the amount present and the ability of a structure to scatter X-rays.

The crystalline phases of glass-ceramic specimens were identified by XRD. The lattice parameters of the N5-type hexagonal unit cell were calculated by a least-squares method using the XRD peaks of (054), (044), (134), (440), and (024).

10.2.2.3 Scanning Electron Microscope and Transmission Electron Microscope

A recent and very useful research tool is a scanning electron microscope (SEM). The surface of a specimen to be examined is scanned with an electron beam, and the reflected (or backscattered) electron beam is collected and then displayed at the same scanning speed on a cathode ray tube (CRT). The image on the screen that may be photographed represents the surface features of the specimen. The surface may or may not be polished and etched but must be electrically conductive. A very thin metal surface coating must be applied to the nonconductive material. Magnifications in the range of 10 times to 50,000 times are also possible, and there is also a very great depth of field. Ancillary equipment allows qualitative and semiquantitative analysis of the elemental composition of highly localized surface areas.

The image seen with a transmission electron microscope (TEM) is formed by an electron beam passing through the specimen. Details of the internal microstructural features are accessible for observation. The contrasts in the image are caused by the differences in beam scattering or diffraction occurring between the various elements of the microstructure or defect. Since the solid materials are highly absorptive to the electron beams, the specimen to be examined must be prepared in the form of a very thin foil. This allows a significant fraction of the incident beam to penetrate the specimen. The transmitted beam is projected onto a fluorescent screen or a photographic film so that the image can be seen.

Glass-ceramics of Y^{3+}-containing Narpsio were subjected to SEM and TEM for microstructural analysis. Electron diffraction and compositional analyses were also performed to characterize the structure of the grain boundary.

10.2.2.4 Arrhenius Plot and Kissinger Plot

In chemical kinetics, an Arrhenius plot displays the logarithm of a reaction rate constant (ln k, ordinate axis) plotted against inverse temperature (1/T, abscissa axis). Arrhenius plots are often used to analyze the effect of temperature on the

rates of chemical reactions. For a single rate-limited thermally activated process, an Arrhenius plot gives a straight line, from which the activation energy can be determined. The temperature dependence Arrhenius plots were presented based on the calculated conductivity values of grains and grain boundaries of the Narpsio glass-ceramics.

Apparent activation energies for crystallization (crystal growth) were determined by employing the non-isothermal-modified Kissinger methods [31, 32] in which some characteristics of the crystallization peak determined by DTA were monitored as a function of heating rate or temperature. The following relationship was then applied.

$$\ln\left(\frac{\alpha^n}{{T_0}^2}\right) = -\frac{\mathrm{E}m}{\mathrm{R}T_0} + const.,$$

where α is the heating rate, T_0 is the peak crystallization temperature at a given heating rate, E is the apparent activation energy, R is the gas constant, and m and n are numerical factors which depend on the crystallization mechanism (m depends on the dimensionality of crystal growth). When bulk crystallization occurs with an increasing number of nuclei (i.e., the number of nuclei is inversely proportional to the heating rate), $m = 3$ and $n = 4$ (indicating three-dimensional growth of crystals). In this study, the parameters m and n were assumed to be 3 and 4, respectively, because bulk glasses were heated to a temperature above ca. 50 °C of T_g in order to obtain homogeneous nucleation.

10.3 Phase Stability and Transformation

10.3.1 Composition Dependence of Precursor and High-Temperature-Stable phases

Figure 10.4 shows the composition dependence of both the precursor phases and the high-temperature-stable phases of glass-ceramic Y-Narpsio on the maps of phosphorus-yttrium (P-Y, Fig. 10.4a), yttrium-sodium (Y-Na, Fig. 10.4b), and phosphorus-sodium (P-Na, Fig. 10.4c), where the variables on the abscissas and ordinals are expressed with the composition parameters $1 - x$, y, and $3 + 3x - y$ for yttrium, phosphorus, and sodium, respectively. As reported before [10, 21], N3- and N9-type Y-Narpsio glass-ceramics can be crystallized as the high-temperature-stable phases at the regions of higher yttrium content [Y] ($1 - x >$ approximately 0.8) and rather lower [Y] ($1 - x <$ approximately 0.55), respectively, in the phosphorus content [P]-[Y] relation.

Concerning the precursor phases, only either N3- or N9-type Y-Narpsio was found in any composition, and N5-type Y-Narpsio was difficult to crystallize from glasses at low temperatures. It is also seen in the P-Y map (Fig. 10.4a) that, under a given [P] (< 0.6), a composition with a higher [Y] gives N3-type Y-Narpsio (open

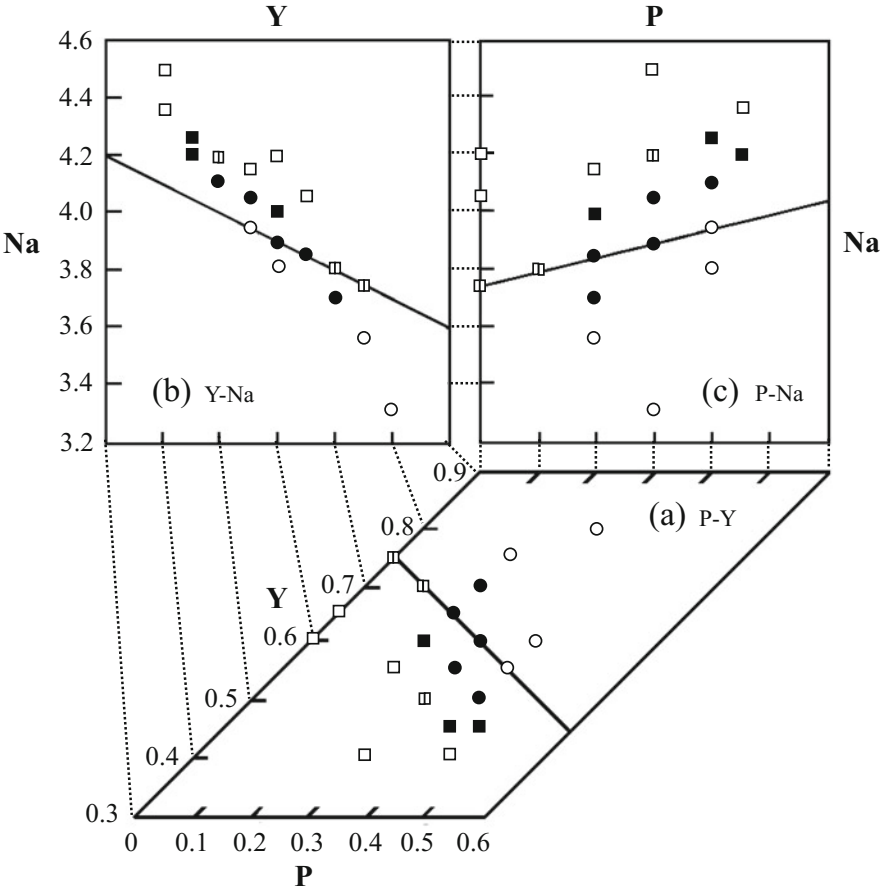

Fig. 10.4 Composition dependence of precursor (pp) and high-temperature-stable phases (sp) of glass-ceramic Narpsio on P-Y (**a**), Y-Na (**b**), and P-Na (**c**) maps, where precursor phases N3 and N9 are shown with circles and squares, respectively. High-temperature-stable phases are shown in such a way that solid marks means that N5-Narpsio is the stable and open marks indicate that the precursor phases are also stable even at high temperatures [30]. Mixed phases are also shown: open circle pp = sp = N3; filled circle pp = N3, sp = N5; open square pp = sp = N9; filled square pp = N9, sp = N5; open split square pp = N9, sp = N9 + N5. Reprinted by permission from Springer Nature: Springer J. Electroceram. 24 (2010) 83, COPYRIGHT (2010)

circles) as the precursor phase, whereas lower [Y] results in N9-type phase (open squares). The values of [Y] dividing the regions allowed for N3- and N9-type Y-Narpsio glass-ceramics decreased with increasing [P], and the boundary seems to locate slightly apart from the deduced line of $[Y] = 0.75 - 0.5[P]$ [10] shown with the solid line. Around the boundary region, N5-type Y-Narpsio can be obtained as the stable phase at high temperatures (solid circles or squares). In the Y-Na or P-Na relations (Fig. 10.4b and c), the region where N5-type Y-Narpsio can be found

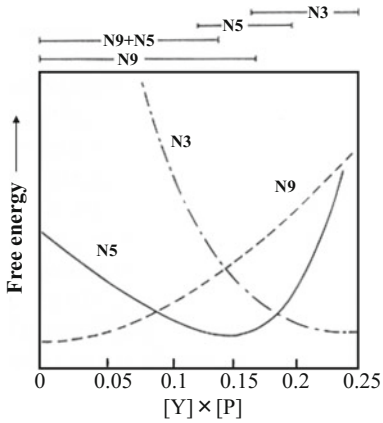

Fig. 10.5 Schematic figure of composition ([Y]×[P]) dependence of free energy of N5-, N3-, and N9-type Y-Narpsio [30]. Reprinted by permission from Springer Nature: Springer J. Electroceram. 24 (2010) 83, COPYRIGHT (2010)

as the high-temperature-stable phase is found under approximately 3.6 < sodium content [Na] < 4.3. The effect of sodium content seems insignificant, because the value of [Na] is subordinately determined as [Na] = 6 − 3[Y] − [P] (=3 +3 $x - y$) depending on the contents of both yttrium and phosphorus.

The above results may suggest that the [P]-[Y] relation dominates the region which is allowed for each Y-Narpsio at high temperatures. Considering this inference, we calculated the products of [P] × [Y] for all the specimens. The values of [P] × [Y] were as follows (shown in Fig. 10.5): 0.16–0.25 for single-phase N3-type Y-Narpsio, 0.14 for mixed phases of N3- and N5-type Y-Narpsio, 0.12–0.20 for single-phase N5-type Y-Narpsio, 0–0.14 for the mixed phases of N5- and N9-type Y-Narpsio, and 0–0.17 for single-phase N9-type Y-Narpsio, respectively. It was therefore deduced (Fig. 10.5) that the free energy of formation (ΔG_f) of N9-type Y-Narpsio would be the lowest in a lower region of [P] × [Y], N5-type Y-Narpsio may have the lowest ΔG_f in a medium [P] × [Y] region, and a higher [P] × [Y] would lower the ΔG_f of N3-type Y-Narpsio.

For a specimen in which N5-type Y-Narpsio is the stable phase at high temperatures, the aspect such as Fig. 10.6a would be illustrated in that ΔG of N3- or N9-type Y-Narpsio would be much smaller than that of N5-type Y-Narpsio near the crystallization temperature (T_c), and the value of N5-type Y-Narpsio would be lowered much less than of the two. Figure 10.6b indicates the aspect that ΔG of N3- or N9-type Y-Narpsio is stable.

10.3.2 Kinetic Effects of Composition on the Phase Transformation

The kinetic effects of composition on the phase transformation are shown in Fig. 10.7, which compares the phase transformation rates of specimens

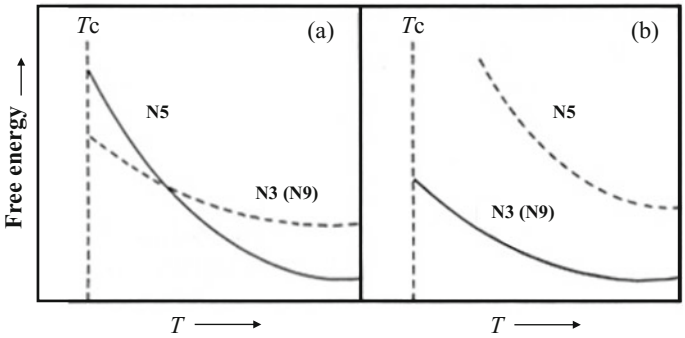

Fig. 10.6 Schematic figures of temperature dependence of free energy change of N5- and N3- or N9-type Y-Narpsio in the cases assuming N5- (**a**) and N3- (**b**) or N9-type (**b**) Y-Narpsio as the high-temperature-stable phase, where *T*c is the crystallization temperature [30]. Reprinted by permission from Springer Nature: Springer J. Electroceram. 24 (2010) 83, COPYRIGHT (2010)

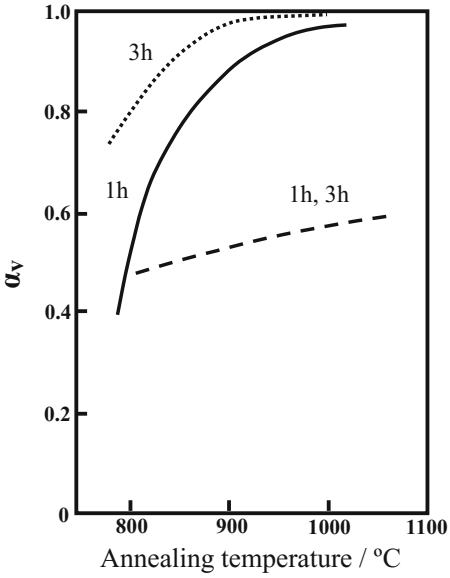

Fig. 10.7 Comparison of phase transformation rate (α_v) between specimens $Na_{3.9}Y_{0.6}P_{0.3}Si_{2.7}O_9$ (1 h-annealing, (—); 3 h-annealing, (· · ·)) and $Na_{3.75}Y_{0.65}P_{0.3}Si_{2.7}O_9$ (1 h, 3 h-annealing, (- - -)) [30]. Reprinted by permission from Springer Nature: Springer J. Electroceram. 24 (2010) 83, COPYRIGHT (2010)

$Na_{3.9}Y_{0.6}P_{0.3}Si_{2.7}O_9$ and $Na_{3.75}Y_{0.65}P_{0.3}Si_{2.7}O_9$. The transformation rate (α_v) of a precursor phase to the stable N5 phase was determined as the weight ratio of N5-type Y-Narpsio in a glass-ceramic specimen. The value of α_v was experimentally obtained from the relationship between the weight ratio and the XRD intensity ratio, which had been determined previously by XRD intensity measurement on specimens with a given weight ratio of N5-type Y-Narpsio to metastable phases. It is seen that the composition $Na_{3.9}Y_{0.6}P_{0.3}Si_{2.7}O_9$ is superior to the other, for

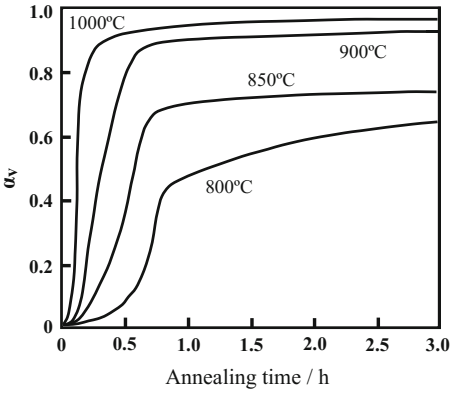

Fig. 10.8 Phase transformation rate (α_v) of N3- to N5-type Y-Narpsio on the specimen $Na_{3.9}Y_{0.6}P_{0.3}Si_{2.7}O_9$ [30]. Reprinted by permission from Springer Nature: Springer J. Electroceram. 24 (2010) 83, COPYRIGHT (2010)

Table 10.1 Kinetic parameters of phase transformation of N3- to N5-type Y-Narpsio of $Na_{3.9}R_{0.6}Si_{2.7}O_9$ [30]

Annealing temp. (K)	Avrami modulus n	ln k
1073	2.61	−20.7
1123	1.94	−14.6
1173	1.39	−9.54
1223	0.75	−4.41

Reprinted by permission from Springer Nature: Springer J. Electroceram. 24 (2010) 83, COPYRIGHT (2010)

the N5 single-phase Y-Narpsio was difficult to obtain in the latter specimen. In specimen $Na_{3.9}Y_{0.6}P_{0.3}Si_{2.7}O_9$, a glass-ceramic of N5 single-phase Y-Narpsio was easily obtained at a temperature higher than 900 °C for only 3 h. The composition $Na_{3.75}Y_{0.75}Si_3O_9$ (or $Na_5YSi_4O_{12}$) was inferior in the same respect.

Figure 10.8 shows the kinetic characteristics of phase transformation of the metastable phase of N3- to N5-type Y-Narpsio of specimen $Na_{3.9}Y_{0.6}P_{0.3}Si_{2.7}O_9$ at various temperatures. The transition rates, α_v, of the silicophosphate Y-Narpsio were much higher than those of the $Na_{3.75}Y_{0.75}Si_3O_9$ silicate material.

The results shown were analyzed with the Avrami empirical equation, $\alpha_v = 1 - \exp(-kt^n)$, where k is the rate constant and n is a constant. The data on α_v obtained at the initial and intermediate stages gave a linear relationship between $\ln(\ln(1 - \alpha_v)^{-1})$ and $\ln(t)$ with a correlation coefficient of more than 0.99. The Avrami parameter and rate constants obtained are summarized in Table 10.1. Based on the Arrhenius relationship (Fig. 10.9), $k = A\exp(-E_v/RT)$ with E_v as the activation energy and constants A and R, where the k values which increased with increasing temperature, we obtained an activation energy of 1.2×10^3 kJ/mol, suggesting that the phase transformation could be rather difficult to take place. An addition of phosphorus and the excess sodium seem effective to the promotion of the phase transformation.

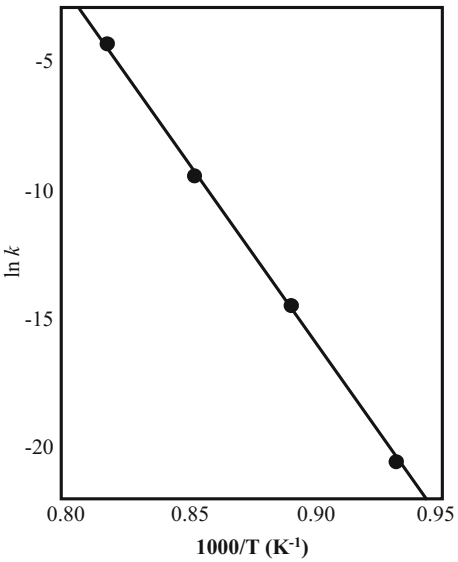

Fig. 10.9 Arrhenius-type plot of ln k with 1000/T of specimen $Na_{3.9}Y_{0.6}Si_{2.7}O_9$ [30]. Reprinted by permission from Springer Nature: Springer J. Electroceram. 24 (2010) 83, COPYRIGHT (2010)

10.4 Effects of Microstructure on Conduction Properties

10.4.1 Crystallization and Phase Diagram

As expected from the previously reported results on Y-Narpsio [9], the crystallization of the superionic conducting N5-type phase took place, depending both on the contents of [R] and [P], at temperatures of 800–1000 °C in most Narpsio glasses of Er to Sm, except for scandium and lanthanum Narpsio glasses. The N5 single-phase region was wider for Narpsio of smaller R but was limited at the [P] $\approx$ 0 region. The effect of phosphorus substitution for Si is important in the crystallization of N5-type phase. Composition 7

$$Na_{3.9}R_{0.6}P_{0.3}Si_{2.7}O_9 \tag{10.7}$$

was experimentally shown as the most appropriate composition for the crystallization of N5-type phase.

The relationship between the ionic radius of R^{3+} (r_R) and the hexagonal lattice parameters of N5-type single phase is consistent with the previous report [4] on $Na_5RSi_4O_{12}$ (R = Sc–Sm) in the tendency that both lattice parameters increased with increasing r_R. The elongation of these lattice axes is attributed to the octahedral coordination of R^{3+} with the O^{2-} of SiO_4- or PO_4-tetrahedra of the 12-membered rings. The local structure around R^{3+} ions is to be further discussed below in relation to conduction properties. On the formation of N5-type single phase, the incorporation of excess sodium ions [$4(3 + 3x - y)/3 - 5 = (12x - 4y - 3)/3$ in

composition 3] and substitution of rare earth ions [$1 - 4(1 - x)/3 = (4x - 1)/3$] must be accounted for in view of the N5-type crystal structure.

Banks et al. [8] have reported the values of σ_{300} as 5×10^{-3} to 1×10^{-2} S/cm for glass-ceramic $Na_5RSi_4O_{12}$ (R = Er, Y, Gd, Sm), which are as low as those of the mixed-phase Narpsio specimens. The single-phase N5-type glass-ceramic was not obtained in the present work. Based on the above crystallization analysis, their glass-ceramic specimens are reasonably considered to suffer from phase inhomogeneity brought about by insufficient annealing. The formation of N5-type structure from the precursor glasses is a matter of crystallization kinetics, because single-phase N5 has been synthesized in single crystal [2, 3, 33] or polycrystalline [6, 7, 11] form based on the composition of N5. It is noted here that the precursor phases identified were N3- or N9-type. Both N3 and N9 are considered to form isostructural [12, 21, 34] with $Ca_3Al_2O_6$ [35] to be comprised of the skeleton structure of six-membered SiO_4-tetrahedra rings [14]. It is generally known that phosphorus pentoxide acts as a nucleating agent in the formation of glass-ceramics. It is therefore presumed at present that the substitution of an asymmetric PO_4-tetrahedron has a weakening effect on the bonding of the skeleton structure of 6-membered SiO_4-tetrahedra rings, resulting in the tendency to form the stable 12-membered structure.

10.4.2 Conduction Properties of Crystalline Grains

The complex impedances and admittances of the measured Narpsio glass-ceramics consisted of two semicircles below 300 °C. The two intercepting points on the real axis are interpreted as the resistance of the crystallized grains (R_G) and the total resistance of grains and remaining glassy grain boundaries (R_{GB}). Figure 10.10 shows examples of the temperature dependence Arrhenius plots based on the calculated conductivity values of grains and grain boundaries of the glass-ceramics Y-Narpsio ($Na_{3.9}Y_{0.6}P_{0.3}Si_{2.7}O_9$) and Sm-Narpsio ($Na_{3.9}Sm_{0.6}P_{0.3}Si_{2.7}O_9$), in which the geometrical ratios of thickness-to-surface area for grains were also used for convenience for those of grain boundaries, because of their undefinable shapes. Table 10.2 summarizes the measured conductivities (σ_{300}) and the calculated activation energies (E_a) assigned for grains of the glass-ceramics with composition 7 of Sc to La, regardless of whether their crystalline phases are N5-type or not. The conductivities, σ_{300}, of single-phase Narpsio specimens of Er to Sc range from 4×10^{-2} to 1×10^{-1} S/cm; in accordance the E_a falls in the range of 23–27 kJ/mol. In contrast, the mixed-phase Narpsio of Sc and In showed much smaller σ_{300} of 3×10^{-3} with an E_a of 35–40 kJ/mol, whereas non-Narpsio glass-ceramics with unknown or mixed phases showed much lower conductivities of 1×10^{-5} to 1×10^{-4} S/cm with an E_a of 55–58 kJ/mol.

The tendency of the conduction properties in single-phase Narpsio specimens is consistent with the reported result measured on the corresponding polycrystalline

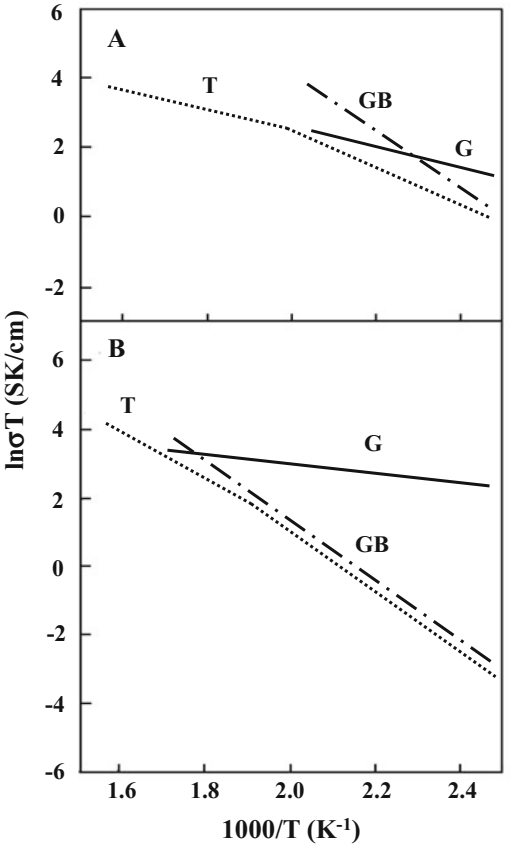

Fig. 10.10 Arrhenius plots of the conductivities of grains (G), grain boundaries (GB) and the total bulk (T) of the glass-ceramic $Na_{3.9}Y_{0.6}P_{0.3}Si_{2.7}O_9$ (A) and $Na_{3.9}P_{0.3}Sm_{0.6}Si_{2.7}O_9$ (B) [30]. Reprinted by permission from Springer Nature: Springer J. Electroceram. 24 (2010) 83, COPYRIGHT (2010)

Table 10.2 Conduction properties of various Narpsio glass-ceramics with composition $Na_{3.9}R_{0.6}Si_{2.7}O_9$ [30]

R^{3+} (ions)	Ea kJ•mol^{-1}	Conductivity (σ_{300}) S•cm^{-1}	Crystalline phase
Sc	35.3	3.2×10^{-3}	N5-type + unknown
In	39.8	3.1×10^{-3}	N5-type + unknown
Er	26.9	3.6×10^{-2}	N5-type
Y	26.6	6.6×10^{-2}	N5-type
Gd	23.0	1.3×10^{-1}	N5-type
Eu	24.4	5.2×10^{-2}	N5-type
Sm	20.9	6.3×10^{-2}	N5-type
Nd	55.1	2.2×10^{-5}	Unknown
La	57.8	1.6×10^{-4}	Unknown

Reprinted by permission from Springer Nature: Springer J. Electroceram. 24 (2010) 83, COPYRIGHT (2010)

$Na_5RSi_4O_{12}$ [4]: σ increased with increasing r_R. Previous works have proposed a mechanism whereby rare earth ions, octahedrally coordinated with the non-bridging oxide ions of the 12-membered rings of silica tetrahedra, work to expand the conduction paths for Na^+ ions along the c-axis [4, 33], which could explain the observed dependence of E_a on r_R in this work.

10.4.3 Structure and Conduction Properties of Grain Boundaries

As R_{GB} decreases rapidly with increasing temperature because of high $(E_a)_{GB}$ to a comparable value with R_G at 300 °C (Fig. 10.10), the total conductivities ($R_G + R_{GB}$) are dominated by grain boundary conductivity. The grain size-dependence of σ_{300} is therefore explained by the decrease in the number of poorly conductive grain boundaries with increasing grain size.

The conduction properties of grain boundaries were strongly dependent on the annealing conditions, although those of the grains were little changed by the annealing temperature and time. Glass-ceramics are generally composites consisting of crystallized grains and small amounts of residual glass (< 1%) [23]. To compare the properties of grain boundaries with those of glasses, the conduction properties of sodium-yttrium silicophosphate glasses with various compositions were measured. Unlike glass-ceramics, the impedance loci of glasses were comprised of one arc, which indicates that there is no polarization arising from microstructural inhomogeneity. Based on the intercepting points on the horizontal axis, the composition dependence of the conduction properties of σ_{300} and E_a was evaluated. The value of σ_{300} ranged from 1×10^{-4} to 5×10^{-3} S/cm, and E_a increased from 53 to 67 kJ/mol with [Na] or [Na]/[Y]. These results are also in good agreement with those reported for the glasses in the Na_2O-Y_2O_3-SiO_2 system [36]. The values of $(E_a)_{GB}$ of the specimens annealed below 950 °C for shorter times correspond to those in the range of glasses, strongly suggesting that their grain boundaries are a glassy matrix. The abovementioned dependence of $(E_a)_{GB}$ on sodium oxide content [Na_2O] is explained by the well-known tendency that the conduction properties of glasses are improved by increasing [Na_2O], which provides the increase in carrier Na^+ ions. The ratio of [Na]/[Y] is also an important parameter for the conduction properties [36], showing an effect on the conduction properties similar to [Na_2O].

In order to identify the structure of the grain boundaries of the specimen ($Na_{3.9}Y_{0.6}P_{0.3}Si_{2.7}O_9$) annealed at 800 °C for 0.5 h, TEM analysis was performed both on grains and grain boundaries. The results in Fig. 10.11 show clear electron diffraction on grains, but not on grain boundaries. This confirms that the grain boundaries are amorphous. Compositional analyses were also performed; however, [Na] was difficult to determine because of the evaporation by electron ablation. It was also observed that the glassy phase was condensed at triple points enclosed by grains and that the neck growth among the grains was well developed. Thus, it is

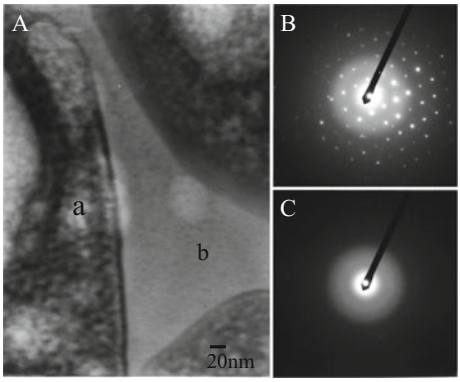

Fig. 10.11 TEM micrograph of glass-ceramic specimen ($Na_{3.9}Y_{0.6}P_{0.3}Si_{2.7}O_9$) annealed at 800 °C for 0.5 h (**a**) and the electron diffraction patterns on the spots a (**b**) and b (**c**) in Fig. 11A [18]. Reprinted with permission from J. Electrochem. Soc., 143, (1996) 2180. Copyright 1996, The Electrochemical Society

reasonable to consider that the grain boundaries annealed at lower temperatures are amorphous, whereas those annealed at higher temperatures for longer periods of time are poorly conductive crystalline compounds in the specimens.

10.5 Microstructural Control of Glass-Ceramic Narpsio Conductors

10.5.1 Preparation of Crack-Free $Na_5YSi_4O_{12}$-Type Glass-Ceramics Containing Large Sm^{3+} Ions: Crystallization Conditions and Ionic Conductivities [15–17]

A number of glass-ceramics of the phosphorus-containing N5-type Na^+ superionic conductors have been prepared by the crystallization of glasses with the composition formula 2, where it was found that the identity of *R* strongly influences the glass crystallization and its conduction properties. To date, polycrystalline N5-type Narpsio compounds have been prepared using Sc, Y, Gd, or Sm as the *R* component. In such compounds, the ionic radius of *R*, which is coordinated to six oxygen atoms, strongly affects the phase crystallization. In addition, the reported results for the silicate ceramics show that the conductivity of N5-type Narpsio increases with an increasing ionic radius of *R*, thereby giving the order Sm-Narpsio > Gd-Narpsio > Y-Narpsio > Sc-Narpsio. However, this order has not always held true in glass-ceramics. Although the majority of Narpsio compounds have been obtained as crack-free bulky glass-ceramics (15 mm diameter and 5 mm thickness), the cracking of Sm-Narpsio during crystallization has proven difficult to prevent. Furthermore, crack-free Gd-Narpsio, which contains relatively large Gd^{3+} ions, was found to be the most conductive; however, Sm-Narpsio, which contains the largest *R* ions, exhibited a lower conductivity than Y-Narpsio, which contained only medium Y^{3+}

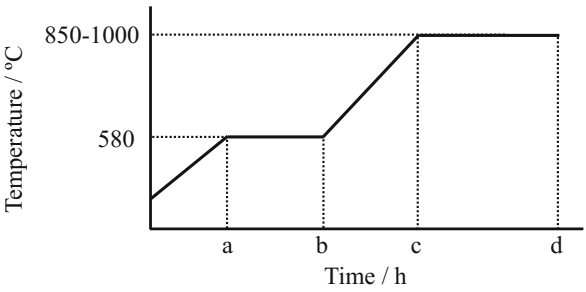

Fig. 10.12 Temperature/time program for the production of the Sm-Narpsio glass-ceramics [17]. Reprinted from J. Ceram. Soc. Jpn. 111 (2003) 257, Copyright 2003

	a-b	b-c	c-d
(A)	1	7	17
(B)	3	8	10
(C)	6	8	5

a-b : Nucleation c-d : Crystal growth

ions. In the study discussed herein, N5-type Sm-Narpsio ionic conductors were prepared by the crystallization of the corresponding glasses, and the optimum conditions for crystallization are discussed in this review with reference to the conduction properties and the preparation of crack-free N5-type glass-ceramic Sm-Narpsio.

Samples were prepared according to the desired composition $Na_{3+3x-y}Sm_{1-x}P_ySi_{3-y}O_9$, and the temperatures employed for nucleation and crystallization of the glass specimens were selected based on the results of DTA. Figure 10.12 shows the temperature/time program employed for preparation of the Sm-Narpsio glass-ceramics. The corresponding N5-type Sm-Narpsio ionic conductors were then produced successfully following the crystallization of these glasses. Although the glass samples heated using program (A) broke during crystallization, and the glass-ceramic Sm-Narpsio obtained using pattern (B) cracked easily during crystallization, the majority of Sm-Narpsio compounds prepared using pattern (C) were obtained as crack-free bulky glass-ceramics. However, it should be noted that the glass samples broke during crystallization when a crystallization heating time of > 5 h was employed. Figure 10.13 shows the phase-composition diagram of the samples crystallized at 900 °C using pattern (C). As indicated, crystallization of the N5 single-phase glass-ceramic Sm-Narpsio was strongly dependent on the concentrations of both *R* and P (or *x* and *y* in the composition parameters) and on the temperature used to crystallize the glass specimens. In addition, Figure 10.14 shows a SEM micrograph of the $Na_{3.9}Sm_{0.6}P_{0.3}Si_{2.7}O_9$ specimen microstructure heated at 900 °C using pattern (C). The grain size of this specimen was approximately 3–5 μm. The state of grain growth was promoted by increasing the crystallization

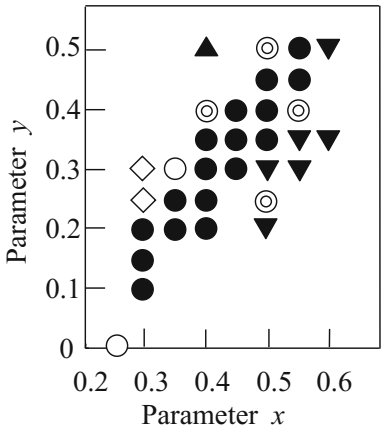

Fig. 10.13 Phase-composition diagram of the Sm-Narpsio glass-ceramics crystallized at 900 °C [17]. • N5, ▲ N3, ▼ N9, ◯N5+N3, ◎N5+N9, ◊N3+N9. Reprinted from J. Ceram. Soc. Jpn. 111 (2003) 257, Copyright 2003

Fig. 10.14 SEM micrograph of the $Na_{3.9}Sm_{0.6}P_{0.3}Si_{2.7}O_9$ specimen heated at 900 °C using heating program (C) [17]. Reprinted from J. Ceram. Soc. Jpn. 111 (2003) 257, Copyright 2003

heating temperature and heating time. Although grain growth can result in high conductivity, crack prevention was difficult in the case of the samples prepared with long heating times. Conduction properties were measured using the alternating current (AC) two-probe method with a low-frequency impedance analyzer. The glass-ceramics for analysis were prepared as cylindrical samples with typical diameters and thicknesses of 15 and 2 mm, respectively. Electrodes were prepared by the sputtering of gold on polished surfaces. The frequency of the applied AC field ranged from 5 to 10 MHz, and the temperature dependence of the conductivity was measured similarly at several temperatures ranging from room temperature to 350 °C. Table 10.3 summarizes the conduction properties of the N5-type glass-ceramic NaSmPSi specimens. It is likely that the low conductivity of Sm-Narpsio (which contained large Sm^{3+} ions) compared to that of Y-Narpsio (containing medium-sized Y^{3+} ions) was due to the particularly small grain sizes of the presented specimens.

Table 10.3 Conduction properties of the N5-type Sm-Narpsio glass-ceramics [17]

Mix proportion		$\sigma_{300}/10^{-1}$ S•cm^{-1}	*E*a/kJ•mol^{-1}		
x	*y*		T	G	G.B.
0.40	0.30	0.238	27.6	17.9	51.4
0.45	0.40	0.408	30.4	18.8	95.7
0.50	0.35	0.352	19.5	15.8	
0.50	0.40	0.478	29.3	16.6	

Heat treatment: 900 °C, 5 h
Reprinted from J. Ceram. Soc. Jpn. 111 (2003) 257, Copyright 2003
σ_{300}: Conductivity at 300 °C
*E*a: Activation energy (*T* total, *G* grain, *G.B.* grain boundary)

10.5.2 Composition Control of Silicophosphate Glass-Ceramics

10.5.2.1 Ionic Conductivities of Nasicon-Type Glass-Ceramic Superionic Conductors in the System Na_2O-Y_2O_3-XO_2-SiO_2 (X = Ti, Ge, Te) [37]

Our phosphorus-containing compositions have been confirmed to be superior to the mother composition of N5, especially in the production of single-phase glass-ceramics. Recently, our work has mainly focused on the synthesis of various glass-ceramics with N5 single phase. In the study discussed herein, N5-type glass-ceramics of the titanium-, germanium-, or tellurium-containing Na^+ superionic conductors (N5Y*X*S) were prepared from glasses with the composition $Na_{3+3x}Y_{1-x}X_ySi_{3-y}O_9$ (X = Ti; NYTiS, Ge; NYGeS, Te; NYTeS) ranging in x = 0.1–0.55 and y = 0.1–0.45, and the effect of the X element on phase separation was investigated along with the effect of the sample microstructure on the conduction properties of the glass-ceramics.

The precursor glasses were prepared by melting stoichiometric mixtures of reagent-grade powders of anhydrous Na_2CO_3, Y_2O_3 (TiO_2, GeO_2, or TeO_2), and SiO_2 at 1300–1400 °C for 1 h, followed by annealing for several hours at an optimum temperature. Following crystallization of the obtained glasses, the corresponding N5Y*X*S ionic conductors were successfully produced. Figures 10.15, 10.16, and 10.17 show the diagrams of phase-composition-crystallization temperature of the obtained NYTiS, NYGeS, and NYTeS glass-ceramics, respectively, where it was apparent that N5Y*X*Si was obtained as a stable phase at high temperatures. In addition, the crystallization of a single N5 phase was found to be strongly dependent on the contents of yttrium and (titanium, germanium, or tellurium) ions (or the values x and y in $Na_{3+3x}Y_{1-x}X_ySi_{3-y}O_9$). Furthermore, the N3 and N9 phases were crystallized as high-temperature-stable phases in the regions of higher Y and rather lower Y concentrations, respectively. The combination of x and y gave the

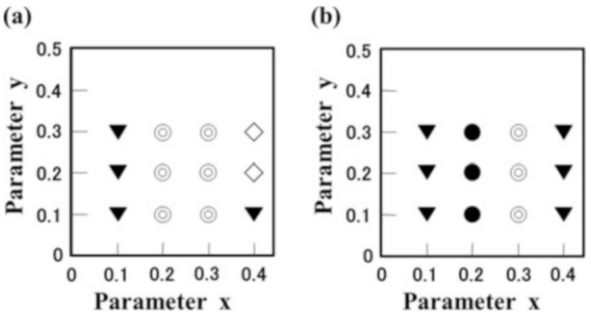

Fig. 10.15
Phase-composition diagrams of the NYTiS glass-ceramics heated at 900 °C (**a**) and 1000 °C (**b**) for 5 h [37]. • N5, ▼ N9, ⊙ N5+N9, ◊ N3+N9. Reprinted from Solid State Ionics 180 (2009) 537, Copyright 2009, with permission from Elsevier

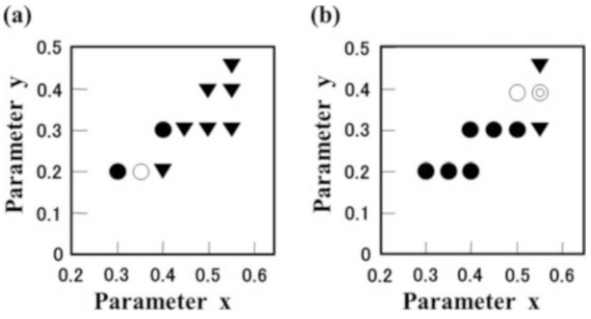

Fig. 10.16
Phase-composition diagrams of the NYGeS glass-ceramics heated at 900 °C (**a**) and 1000 °C (**b**) for 5 h [37]. • N5, ▼ N9, ◯ N5+N3, ⊙ N5+N9. Reprinted from Solid State Ionics 180 (2009) 537, Copyright 2009, with permission from Elsevier

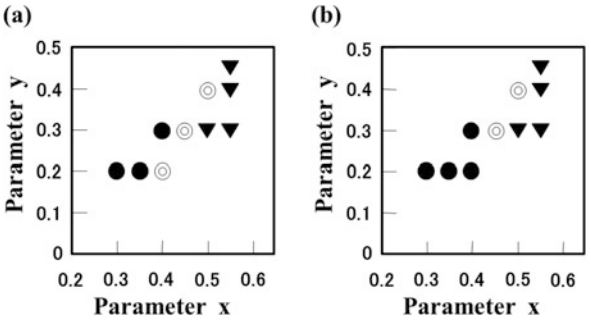

Fig. 10.17
Phase-composition diagrams of the NYTeS glass-ceramics heated at 900 °C (**a**) and 1000 °C (**b**) for 5 h [37]. • N5, ▼ N9, ⊙ N5+N9. Reprinted from Solid State Ionics 180 (2009) 537, Copyright 2009, with permission from Elsevier

greatest variation in N5YGeS but was more limited in the order: N5YTeS > N5YTiS. Moreover, Table 10.4 summarizes the conduction properties of the N5-type glass-ceramics with compositions of $Na_{3.6}Y_{0.8}Ti_{0.2}Si_{2.8}O_9$, $Na_{4.2}Y_{0.6}Ge_{0.3}Si_{2.7}O_9$, and $Na_{4.2}Y_{0.6}Te_{0.3}Si_{2.7}O_9$, respectively. The conductivities and activation energies of these species are in the order of 10^{-2} S/cm at 300 °C and 15–24 kJ/mol, respectively. Interestingly, the conductivity of these samples decreased, giving the order N5YGeS > N5YTeS > N5YTiS. It is considered that this order corresponds to the N5 single-phase region.

Table 10.4 Conduction properties of the N5 glass-ceramics with the $Na_{3.6}Y_{0.8}Ti_{0.2}Si_{2.8}O_9$, $Na_{4.2}Y_{0.6}Ge_{0.3}Si_{2.7}O_9$, and $Na_{4.2}Y_{0.6}Te_{0.3}Si_{2.7}O_9$ compositions [37]

Specimen	Heat treatment		σ_{300}	*E*a/kJ•mol^{-1}		
	Temp.	Time	/10^{-2}•S•cm^{-1}	T	G	G.B.
NYTiS	1000	5	2.5	15.5	19.8	10.0
NYGeS	900	5	4.0	21.1	17.3	44.0
	1000	5	4.5	24.1	19.3	56.6
	1000	24	6.7	22.9	20.6	67.2
NYTeS	900	5	3.2	19.8	18.7	43.7
	1000	5	4.6	21.8	20.5	56.6

Reprinted from Solid State Ionics 180 (2009) 537, Copyright 2009, with permission from Elsevier
σ_{300}: Conductivity at 300 °C
*E*a: Activation energy (*T* total, *G* grain, *G.B.* grain boundary)

10.5.2.2 Synthesis and Na^+ Conduction Properties of Nasicon-Type Glass-Ceramics in the System Na_2O-Y_2O_3-X_2O_3-SiO_2 (X = B, Al, Ga) and Effect of Si Substitution [38]

Following preparation of the glass-ceramics of the boron-, aluminum-, or gallium-containing $Na_5RSi_4O_{12}$-type (R = rare earth; Y) Na^+ superionic conductors obtained from glasses with the $Na_{3+3x+y}Y_{1-x}X_ySi_{3-y}O_9$ composition (X = B; NYBS, X = Al; NYAlS, X = Ga; NYGaS) ($x = 0.2$, $y = 0.1$), the effect of X on the phase separation was investigated in addition to the effect of the microstructure on the conduction properties of glass-ceramics, and the crystallization kinetics of the glasses were examined by DTA.

The precursor glasses were obtained by melting stoichiometric mixtures of reagent-grade powders of anhydrous Na_2CO_3, Y_2O_3 (H_3BO_3, Al_2O_3, or Ga_2O_3), and SiO_2 at 1350 °C for 1 h after calcinations at 900 °C for 1 h. The melts were quickly poured into a graphite cylinder. Crystallization was carried out according to a previous report [14]. The N5-type glass-ceramic NYBS, NYAlS, and NYGaS with the $Na_{3.7}Y_{0.8}B_{0.1}Si_{2.9}O_9$, $Na_{3.7}Y_{0.8}Al_{0.1}Si_{2.9}O_9$, and $Na_{3.7}Y_{0.8}Ga_{0.1}Si_{2.9}O_9$ compositions, respectively, were successfully produced by crystallization of the glasses. The apparent activation energies for crystallization (crystal growth) were determined by employing the non-isothermal-modified Kissinger methods [39, 40], in which some characteristic of the crystallization peak determined by DTA is monitored as a function of the heating rate or temperature. Figure 10.18 shows the modified Kissinger plots for NYBS, NYAlS, and NYGaS glasses. Table 10.5 summarizes the DTA peak temperatures and activation energies of crystal growth obtained from the modified Kissinger equation under non-isothermal condition of the NY*X*S glasses. The activation energies of crystal growth are 410 for NYBS, 392 for NYAlS, and 381 kJ/mol for NYGaS. The activation energy of crystal growth of the NY*X*S glass decreases as the ionic radius of X increases. Table 10.6 summarizes

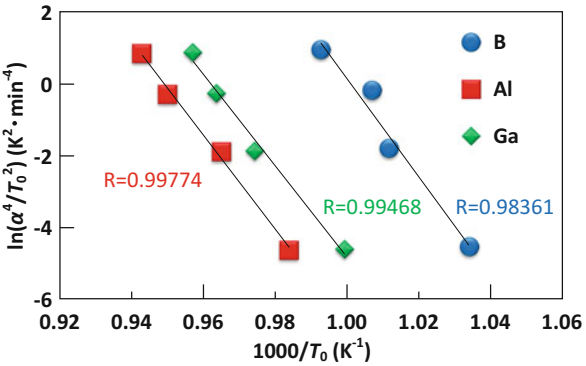

Fig. 10.18 Modified Kissinger plots for the NaYBS, NaYAlS, and NaYGaS glasses [38]. Reprinted from Solid State Ionics 225 (2012) 367, Copyright 2012, with permission from Elsevier

Table 10.5 DTA peak temperatures and activation energies of crystal growth of the NYBS, NYAlS, and NYGaS glasses [38]

	DTA peak temperature (°C)		
Heating rate (°C•min^{-1})	NYBS	NYAlS	NYGaS
10	694	743	728
20	715	763	753
30	720	779	765
40	734	787	772
Activation energy of crystal growth (kJ•mol^{-1})	410	392	382
Ionic radius (nm)	0.025	0.053	0.061

Reprinted from Solid State Ionics 225 (2012) 367, Copyright 2012, with permission from Elsevier

Table 10.6 Conduction properties of the NYBS, NaYAlSi, and NYGaS glass-ceramics [38]

	NYBS	NYAlS	NYGaS
$\sigma_{300\ (G)}$ (S)	5.61×10^{-2}	4.03×10^{-2}	3.79×10^{-2}
$\sigma_{300\ (G.B.)}$ (S)	18.8×10^{-2}	50.4×10^{-2}	33.0×10^{-2}
$\sigma_{300\ (Total)}$ (S)	4.32×10^{-2}	3.73×10^{-2}	3.40×10^{-2}
$Ea_{\ (Total)}$ (kJ•mol^{-1})	12.6	12.8	13.2
Ionic radius (nm)	0.025	0.053	0.061

Reprinted from Solid State Ionics 225 (2012) 367, Copyright 2012, with permission from Elsevier
σ_{300}: Conductivity at 300 °C (*T* total, *G* grain, *G.B.* grain boundary)
Ea: Activation energy at higher temperatures ranging from 250 to 350 °C

the conduction properties of the NY*X*S glass-ceramics. The conductivities of the glass-ceramics NYBS, NYAlS, and NYGaS were 4.32×10^{-2}, 3.73×10^{-2}, and 3.40×10^{-2} S/cm at 300 °C, respectively. The conductivity decreases in the order NYBS > NYAlS > NYGaS. The conductivity of the NY*X*S glass-ceramics decreases as the ionic radius of *X* increases.

10.5.2.3 Effect of Substitution of Si with V and Mo on Ionic Conductivity of $Na_5YSi_4O_{12}$-Type Glass-Ceramics [41]

Glass-ceramics of the vanadium- or molybdenum-containing N5-type Na^+ superionic conductors were prepared by crystallization of glasses with the compositions $Na_{3+3x-y}Y_{1-x}V_ySi_{3-y}O_9$ (NYVS) or $Na_{3+3x-2y}Y_{1-x}Mo_ySi_{3-y}O_9$ (NYMoS) ranging in $x = 0.3$–0.5 and $y = 0.1$–0.4, and the effects of V or Mo elements on the phase separation and the microstructural effects on the conduction properties of glass-ceramics are discussed.

The precursor glasses were made by melting stoichiometric mixtures of reagent-grade powders of anhydrous Na_2CO_3, Y_2O_3, V_2O_5, MoO_3, and SiO_2 at 1400 °C for 1 h, followed by annealing for several hours at an optimum temperature. Figure 10.19 shows the diagrams of phase-composition-crystallization temperature of the glass-ceramic specimens with the $Na_{3.9}Y_{0.6}V_{0.3}Si_{2.7}O_9$ (A) and $Na_{3.7}Y_{0.7}Mo_{0.1}Si_{2.9}O_9$ (B) compositions. N5-type NYVS and NYMoS are obtained as a stable phase at high temperatures. The crystallization of N5 single phase is strongly dependent both on the contents of yttrium and (vanadium or molybdenum) ions (or the values x and y correspond to the composition parameters in $Na_{3+3x-y}Y_{1-x}V_ySi_{3-y}O_9$ or $Na_{3+3x-2y}Y_{1-x}Mo_ySi_{3-y}O_9$). N3 and N9 phases can

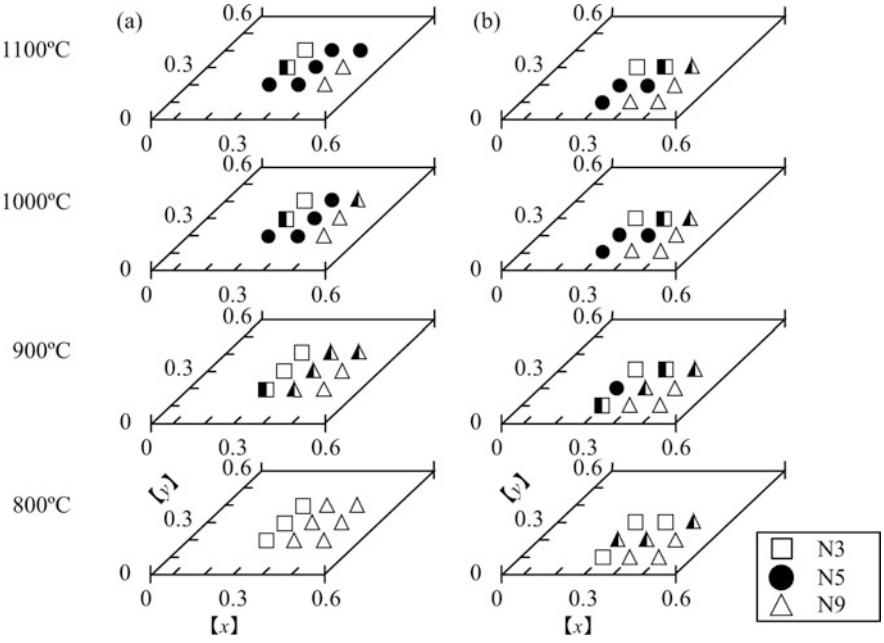

Fig. 10.19 Phase-composition–crystallization temperature diagrams of the NYVS (**a**) and NYMoS (**b**) glass-ceramics crystallized at 800–1100 °C [41]. • N5, □ N3, △ N9, □ $N5^+N3$, △ $N5^+N9$. Reprinted from Solid State Ionics 179 (2008) 1291, Copyright 2008, with permission from Elsevier

Table 10.7 Total conductivities and activation energies of the glass-ceramic specimens $Na_{3.9}Y_{0.6}V_{0.3}Si_{2.7}O_9$ (A) and $Na_{3.7}Y_{0.7}Mo_{0.1}Si_{2.9}O_9$ (B) [41]

(A)						
Temp. (°C)	σ (10^{-2}•S•cm^{-1})			*E*a (kJ•mol^{-1})		
	T	G	G.B.	T	G	G.B.
150	0.13	0.43	0.19			
200	0.28	0.44	0.73	27.5	10.5	47.1
250	0.47	0.62	1.97	——	——	——
300	0.87	1.24	2.93	38.1	40.5	31.7
350	1.63	2.33	5.38			
(B)						
150	0.63	1.24	1.27			
200	1.45	2.11	4.68	29.2		41.1
250	2.46	3.33	9.45	——	22.5	——
300	3.58	4.81	13.91	21.8		19.1
350	4.61	6.49	15.95			

Reprinted from Solid State Ionics 179 (2008) 1291, Copyright 2008, with permission from Elsevier
σ Conductivity, *E*a Activation energy, *T* Total, *G* grain, *G.B.* grain boundary

be crystallized as the high-temperature-stable phases at the regions of rather lower [Y] and higher [Y], respectively. The total conductivities and the activation energies are summarized in Table 10.7. The total conductivities of the specimens (A) and (B) were 0.87×10^{-2} and 3.58×10^{-2} S/cm at 300 °C, respectively, and the activation energies of those specimens were 38.1 and 21.8 kJ/mol, respectively. The combination of x and y was most varied in N5-type NYPS and more limited in N5-type NYVS and NYMoS. The conductivity decreases in the order NYPS > NYMoS > NYVS. It is considered that this order corresponds to the N5 single-phase region. We assume that the effect of the substitution of Si with V or Mo should be to bring about the difference in homogeneity in the N5 ring structure. The total and electronic conductivities and the Na^+ ionic transport numbers of the specimen (A) determined by the Wagner polarization method are summarized in Table 10.8. The ionic transport numbers of specimen (A) were nearly 0.9, and those of specimen (B) were nearly 1. It is considered that approximately 10% of the total conduction is electronic conduction (hopping conduction by transition metal vanadium) in the specimen (A). This result can explain the following fact: the conductivity of the specimen (A) is lower than other N5 conductors.

10.5.2.4 Synthesis and Na^+ Conduction Properties of Nasicon-Type Glass-Ceramics in the System Na_2O-Y_2O_3-R_2O_3-P_2O_5-SiO_2 (R = rare earth) and Effect of Y Substitution [42]

Glass-ceramics of the phosphorus-containing N5-type Na^+-superionic conductors were prepared by the crystallization of glasses of the $Na_{3+3x+y}Y_{1-x-z}R_zP_ySi_{3-y}O_9$

Table 10.8 Total and electronic conductivities and the Na^+ ionic transport numbers of the glass-ceramic specimen $Na_{3.9}Y_{0.6}V_{0.3}Si_{2.7}O_9$ (A) [41]

Temp. (°C)	σ_t (S•cm^{-1})	σ_e (S•cm^{-1})	t_i
150	1.312×10^{-3}	1.582×10^{-5}	0.988
200	2.752×10^{-3}	1.826×10^{-4}	0.934
250	4.728×10^{-3}	4.687×10^{-4}	0.901
300	8.715×10^{-3}	6.582×10^{-4}	0.924
350	1.627×10^{-2}	1.563×10^{-3}	0.904

Reprinted from Solid State Ionics 179 (2008) 1291, Copyright 2008, with permission from Elsevier
σ_t Total conductivity, σ_e Electronic conductivity, t_i Ionic transport number

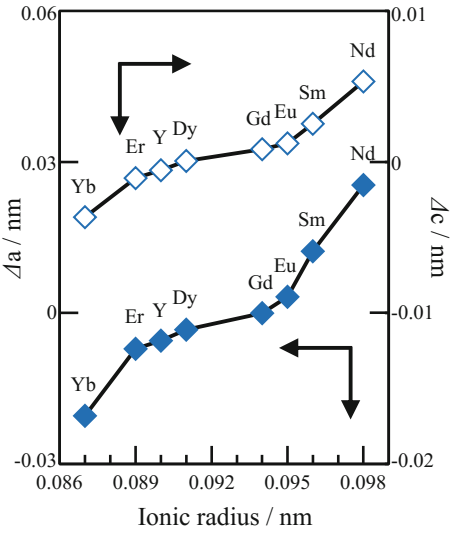

Fig. 10.20 Lattice constants of the NY*R*PS (*R* = Nd, Sm, Eu, Gd, Dy, Er, or Yb) and NYPS (Y-Narpsio) glass-ceramics [42]. Reprinted from Solid State Ionics 262 (2014) 604, Copyright 2014, with permission from Elsevier

composition (NY*R*PS; *R* = Nd, Sm, Eu, Gd, Dy, Er, or Yb, $x = 0.4$, $y = 0.2$, $z = 0.1$), where yttrium was substituted with the various *R* elements. The crystallization kinetics of the glasses were examined by DTA, and the effects of *R* on the phase separation properties of the glass-ceramics were investigated in addition to the effects of the microstructure on the conduction properties.

The precursor glasses were initially prepared by melting stoichiometric mixtures of reagent-grade powders of anhydrous Na_2CO_3, Y_2O_3, R_2O_3 (*R* = Nd, Sm, Eu, Gd, Dy, Er, or Yb), $NH_4H_2PO_4$, and SiO_2 at 1350 °C for 1 h following calcinations at 400 °C for 0.5 h and at 900 °C for 0.5 h. The N5-type glass-ceramics NY*R*PS and NYPS (Y-Narpsio) with the $Na_{4.4}Y_{0.6}P_{0.2}Si_{2.8}O_9$ composition were successfully synthesized by crystallization of the glasses. As indicated in Fig. 10.20, the lattice constants of the glass-ceramic NY*R*PS species increased upon increasing the ionic radius of *R*, whereas the activation energies for crystal growth of the NY*R*PS glass decreased with greater ionic radii (Fig. 10.21). The formation of N5-type structures from the precursor glasses was also found to be dependent on the crystallization kinetics. In this case, the substitution of large *R* ions weakens the bonding of the N3-

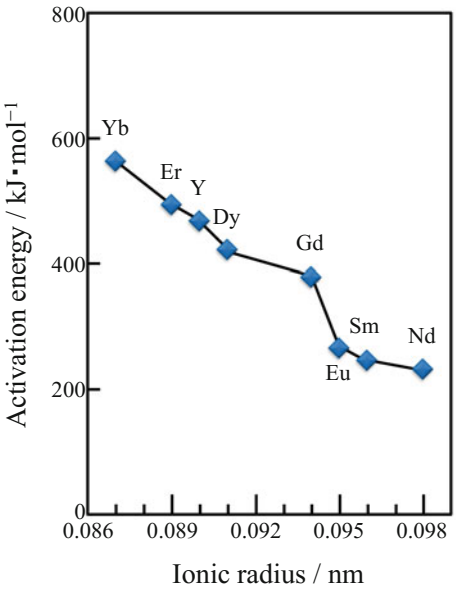

Fig. 10.21 Activation energies (*Ea*) of crystal growth for the NY*R*PS (*R* = Nd, Sm, Eu, Gd, Dy, Er, or Yb) and NYPS (Y-Narpsio) glasses [42]. Reprinted from Solid State Ionics 262 (2014) 604, Copyright 2014, with permission from Elsevier

or N9-type skeleton structure of the 6-membered SiO_4-tetrahedral rings, thereby leading to the formation of stable N5-type 12-membered structure. Furthermore, as shown in Fig. 10.22, the conductivities of the NY*R*PS glass-ceramics increased upon increasing the ionic radius of *R*. Presumably, rare earth ions that are octahedrally coordinated with the non-bridging oxide ions of the 12-membered rings of the silica tetrahedra expand the conduction paths for Na^+ ions along the *c*-axis [4]; this expansion explains the observed dependence of the activation energies on the ionic radius of *R*.

10.5.3 Ionic Conductivities of Na^+ Ion-Implanted Silicophosphate Glass-Ceramics [26]

We consider that a material processing technique to introduce a large number of mobile Na^+ ions into samples is required to realize the superionic conduction in the N5-type Narpsio compounds. Here, we report that a large enhancement in the electrical conductivity, probably due to Na^+ ions, has been obtained in the glass-ceramic Narpsio by ion implantation of Na^+ ions.

Substrate N5-type Narpsio compounds used for ion implantation were the glass-ceramic $Na_{3.9}Y_{0.6}P_{0.3}Si_{2.7}O_9$ and $Na_{3.9}Sm_{0.6}P_{0.3}Si_{2.7}O_9$. Approximately 5-mm-thick glass-ceramic disks were implanted with 200 keV Na^+ ions with flux densities of 10^{14} to 10^{15} ions/cm^2 at room temperature. The current density was 3 $\mu A/cm^2$. The XRD patterns of the Na^+ ion-implanted specimens exhibited

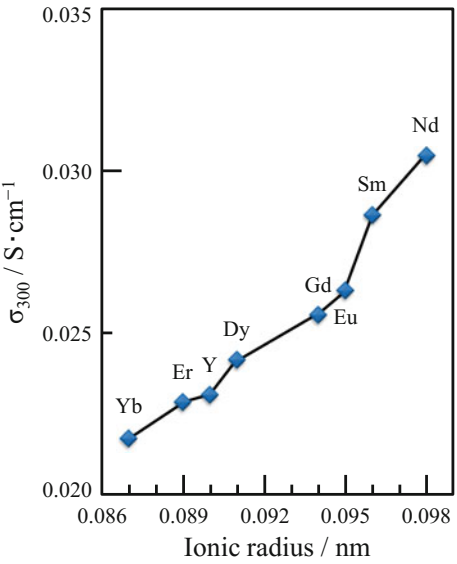

Fig. 10.22 Conductivity at 300 °C of the NY*R*PS (*R* = Nd, Sm, Eu, Gd, Dy, Er, or Yb) and NYPS (Y-Narpsio) glass-ceramics [42]. Reprinted from Solid State Ionics 262 (2014) 604, Copyright 2014, with permission from Elsevier

Table 10.9 Conduction properties of the Na^+-ion-implanted Narpsio glass-ceramics [26]

Dose/ions•cm^{-2}	$\sigma_{300}/10^{-1}$ S•cm^{-1}	*E*a / kJ•mol^{-1}		
		T	G	G.B.
$Na_{3.9}Y_{0.6}P_{0.3}Si_{2.7}O_9$				
Before implantation	0.201	23.8	18.4	31.3
10^{14}	0.427	18.3	13.3	32.2
10^{15}	0.586	19.3	12.6	40.1
$Na_{3.9}Sm_{0.6}P_{0.3}Si_{2.7}O_9$				
Before implantation	0.238	27.6	17.9	51.4
10^{14}	0.512	36.7	16.9	88.8
10^{15}	0.715	33.3	16.3	104.1

Reprinted from Solid State Ionics 136/137 (2000) 1049, Copyright 2000, with permission from Elsevier

σ_{300}, Conductivity at 300 °C

*E*a Activation energy (*T* total, *G* grain, *G.B.* grain boundary)

N5 single phase. No cracking was perceived for any of the implanted surfaces. Table 10.9 summarizes the conduction properties of the glass-ceramic Narpsio specimens. The samples with the $Na_{3.9}Y_{0.6}P_{0.3}Si_{2.7}O_9$ and $Na_{3.9}Sm_{0.6}P_{0.3}Si_{2.7}O_9$ compositions crystallized at 900 °C for 5 h showed the ionic conductivities of 2.01×10^{-2} and 2.38×10^{-2} S/cm at 300 °C, respectively. It was found that Sm-Narpsio containing the largest Sm^{3+} ions was more conductive than Y-Narpsio with medium Y^{3+} ions under the same heating conditions. The ionic conductivities of the glass-ceramic $Na_{3.9}Y_{0.6}P_{0.3}Si_{2.7}O_9$ and $Na_{3.9}Sm_{0.6}P_{0.3}Si_{2.7}O_9$ at 300 °C were drastically enhanced from 2.01×10^{-2} S/cm to 5.86×10^{-2} S/cm and from

2.38×10^{-2} S/cm to 7.15×10^{-2} S/cm, respectively, upon implantation of 200 keV Na^+ ions with a flux density of 10^{15} ions/cm^2.

10.5.4 Structure and Conduction Properties of $Na_5YSi_4O_{12}$-Type Glass-Ceramics Synthesized by Bias Crystallization of Glass [27]

Glass-ceramics of the phosphorus-containing N5-type Na^+ superionic conductors were prepared by bias crystallization of glasses with the composition $Na_{4.05}Y_{0.55}P_{0.3}Si_{2.7}O_9$ in an electric field. The conditions for bias crystallization are discussed with respect to the microstructure and the conduction properties.

The precursor glasses were made by melting stoichiometric mixtures of reagent-grade powders of anhydrous Na_2CO_3, Y_2O_3, SiO_2, and $NH_4H_2PO_4$ at 1350 °C for 1 h, followed by annealing for several hours at an optimum temperature. The annealed specimens were heated to 900 °C in an electric field for the bias crystallization. The thermostable heating holder was produced in order to do the crystallization in a direct current electric field. This holder is made of alumina and platinum. Glass samples (5 mm × 5 mm × 8 mm) were held between the platinum plates and crystallized in an electrical field of 1 V/mm. The thermal treatment was the same as that used in conventional crystallization without the electric field.

The microstructure was investigated with SEM. The grain length of the cross section parallel with the electric field direction was 10–15 nm, and it was proven to be smaller than the 15–30 nm grain length of the cross section perpendicular to the direction and the specimen crystallized by the conventional method. It was possible to control shape and orientation of crystal grain by the crystallization in the electrical field.

Owing to the bias field, an electric current related to temperature was measured during the crystallization process. Figure 10.23 shows a current profile with respect to temperature during the crystallization process in the electric field. The largest observed current was 250 μA. The current profile exhibits three peaks at approximately 600 °C, 700 °C, and 850 °C. These temperatures correspond to those of nucleation, phase transition from N3 phase to N5 phase, and crystallization of glass specimens determined by DTA analysis, respectively. An electric current with respect to temperature was measured newly by applying the bias voltage only in two limited temperature ranges, because two main peaks were observed in Fig. 10.23. One range is from right before of the first main peak (511–652 °C), and another range is from right before of the second main peak (790–865 °C). The resulting current profile is shown in Fig. 10.24. It was found that the mass transfer in the specimen is generated even in the condition of no applied voltage.

Crystalline phases were identified on the sample after the crystallization in the electric field by XRD in order to consider the possibility of structural changes by the movement of Na^+ ion, which is a carrier. In the several cut sections, no difference in

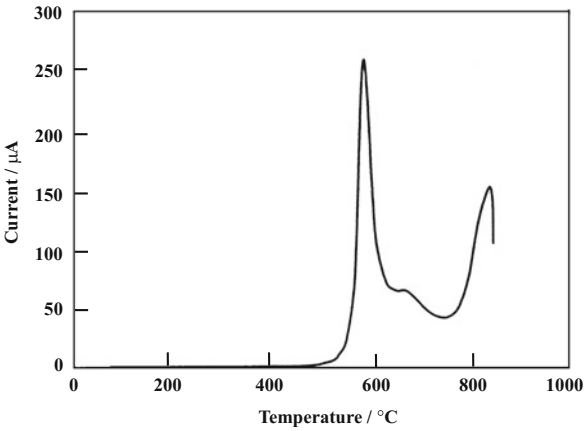

Fig. 10.23 Current profile in relation to temperature during crystallization process in electric field [27]. Reprinted from Solid State Ionics 154 (2002) 361, Copyright 2002, with permission from Elsevier

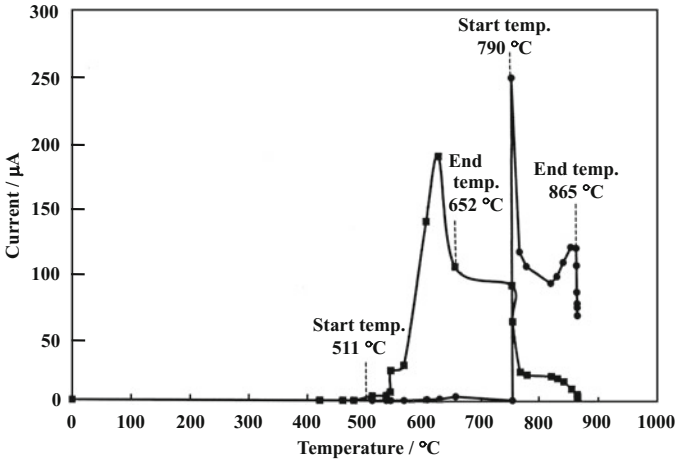

Fig. 10.24 Current profile in relation to temperature measured by applying voltage in two limited temperature ranges [27] Reprinted from Solid State Ionics 154 (2002) 361, Copyright 2002, with permission from Elsevier

the fundamental structure was observed. Judging from the patterns, the N5 single-phase ionic conductors were successfully produced by the bias crystallization of glasses.

Figure 10.25 shows the temperature dependence Arrhenius plots of the conductivities of various specimens. The complex admittances of the measured glass-ceramics consisted of two semicircles below 300 °C. The two intercepting points on the real axis are interpreted as the resistance of the crystallized grains (R_G) and the total resistance of the grains and remaining glassy grain boundaries (R_{GB}). As R_{GB} decreases rapidly with increasing temperature because of high $(Ea)_{GB}$ to a comparable value with R_G at 300 °C, the total conductivities (R_G+R_{GB}) are

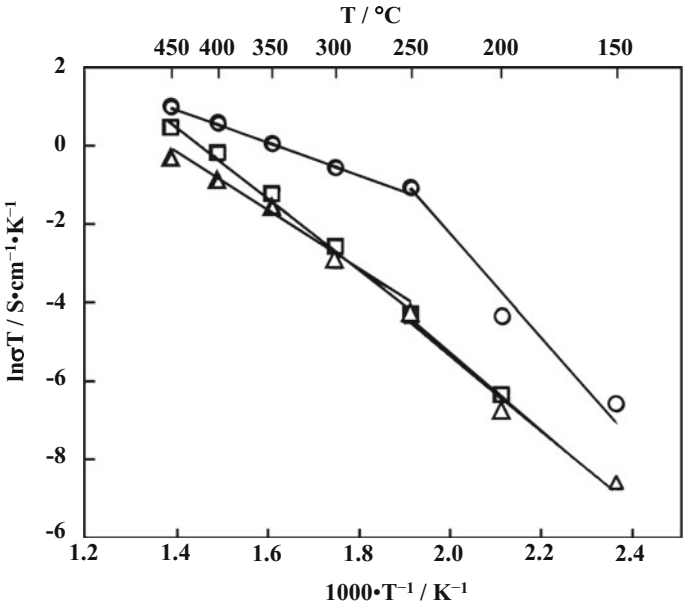

Fig. 10.25 Temperature dependence Arrhenius plots of the conductivities of the bias-crystallized Narpsio glasses [27]. ◯ Conventional, △ Parallel, □ Perpendicular. Reprinted from Solid State Ionics 154 (2002) 361, Copyright 2002, with permission from Elsevier

Table 10.10 Conduction properties of the bias-crystallized Narpsio glasses [27]

	Ea / kJ•mol^{-1}		σ_{300} / mS•cm^{-1}
	Temperature		
	High	Low	
○ Conventional	33.0	99.9	0.9860
△ Parallel	66.6	73.5	0.0923
□ Perpendicular	76.4	82.2	0.1320

Reprinted from Solid State Ionics 154 (2002) 361, Copyright 2002, with permission from Elsevier

dominated by grain boundary conductivity. The effect of the grain boundary is greatly seen on the appearance at lower temperatures. Table 10.10 summarizes the conduction properties obtained from Fig. 10.25. The cross sections parallel and perpendicular to the electric field direction showed the ionic conductivities of 0.0923 and 0.132 mS/cm at 300 °C, respectively. It was found that the bias-crystallized specimens were less conductive than those crystallized by the conventional method. Figure 10.26 shows the temperature dependence of the conductivity of the bias-crystallized specimen. At temperatures over 300 °C, anisotropy in the conductivity was observed. It was also found that the cross section perpendicular to the electric field direction was more conductive than that parallel with the electric field direction. The microstructure and the electric conductivity of the Narpsio glass-

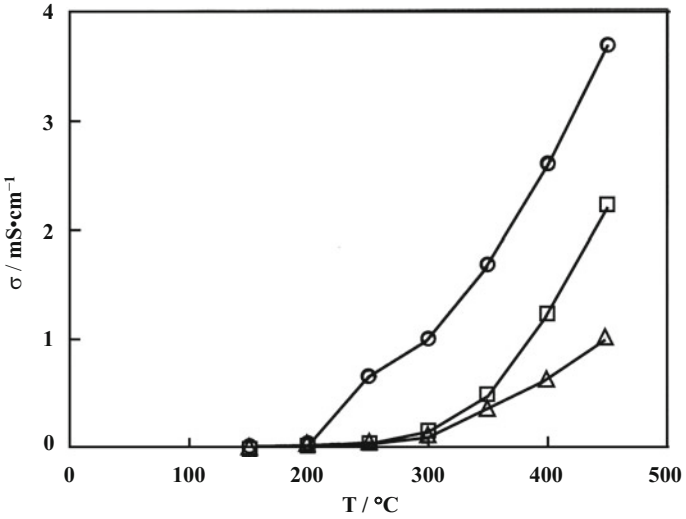

Fig. 10.26 Temperature dependence of conductivity of the bias-crystallized Narpsio glasses [27]. Reprinted from Solid State Ionics 154 (2002) 361, Copyright 2002, with permission from Elsevier

ceramics perpendicular to the electric field direction were significantly different from those in parallel.

10.6 Concluding Remarks

In this article, Na^+ superionic conducting Narpsio glass-ceramics with the $Na_5YSi_4O_{12}$ (N5)-type structure and containing various rare earth elements (R), which were prepared according to the $Na_{3+3x-y}R_{1-x}P_ySi_{3-y}O_9$ composition, were reviewed, and recent research into the structural control of Na^+ superionic conducting glass-ceramics was introduced. The possible combinations of x and y became more limited for the crystallization of the superionic conducting phase as the ionic radius of R increased and the Na^+ conduction properties were more enhanced in the glass-ceramics of larger R. The meaning of the composition formula can be clarified in the thermodynamic and kinetic study of the crystallization and phase transformation of metastable to stable phase in the production of N5-type glass-ceramics. It was demonstrated that the medium value of content product as $[P]\times[R]$ is important in the crystallization of the N5 single phase. The conduction properties of these glass-ceramics were strongly dependent upon the crystallization conditions as well as the compositions. Not only complex impedance analysis but also TEM observations confirmed that this dependence was attributed to the conduction properties of grain boundaries, which were glasses condensed at triple points enclosed by grains.

The Narpsio conductors exhibit great potential and are one of the most important groups of solid electrolytes, not only because they are practically useful for application in advanced batteries but also because they are three-dimensional ionic conductors with a 12-$(SiO_4)^{4-}$-tetrahedra-containing skeleton structure from which, or by analogy with which, various solid electrolyte materials can be derived. In addition, various modified Narpsio glass-ceramics have been synthesized by replacing *R* with Sc, Y, In, La, Nd, Sm, Eu, Gd, Dy, Er, or Yb and/or by substituting tetravalent (Ti^{4+}, Ge^{4+}, Te^{4+}), trivalent (B^{3+}, Al^{3+}, Ga^{3+}), pentavalent (V^{5+}), and hexavalent (Mo^{6+}) ions for P or Si. In this review, the results of Na^+ ion implantation as a material processing technique to introduce a large number of mobile Na^+ ions were presented. A large enhancement in electrical conductivity was observed in the Narpsio glass-ceramics by ion implantation of Na^+ ions. Such glass-making processing is favorable for the fabrication of differently shaped electrolytes, and the microstructures of glass-ceramic electrolytes can be controlled through variation of the crystallization conditions. We have successfully produced anisotropic glass-ceramic conductors by bias crystallization of the glasses in an electric field. The microstructure and the conduction properties were dependent on the current direction in the crystallization process.

10.7 Future Prospects

The Narpsio family has great potential. It is a solid solution in the Na_2O-R_2O_3-P_2O_5-SiO_2 system and is expected to develop a variety of modified Narpsios. Our main work has recently been focused on the synthesis of various glass-ceramics with N5 single phase as shown in Fig. 10.27, which contain 15.6% mobile Na^+ ions and 84.4% bonding Na^+ ions. In the research currently underway, we are trying to synthesize them without *R* elements but with Fe of high abundance and low costs, by melt quenching and glass-crystallization method. Furthermore, mobile Na^+ ions in the N5 phase also can be exchanged for proton or several alkali ions. Our group is advancing the development of new Narpsio family conductors by exchange of carrier mobile Na^+ with Li^+, K^+, or H^+. In the future, we are expecting computational chemistry to elucidate the conduction mechanism in conductors with various kinds of carrier ions.

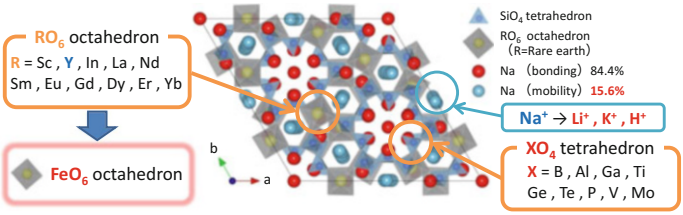

Fig. 10.27 A variety of modified Narpsios

References

1. S. Morimoto, J. Ceram. Soc. Jpn. **97**, 1097 (1989)
2. B.A. Maksimov, Y.A. Kharitonov, A.N.V. Belov, Sov. Phys. Dokl. **18**, 763 (1974)
3. B.A. Maksimov, I.V. Petrov, A. Rabenau, H. Schulz, Solid State Ionics **6**, 195 (1982)
4. T. Okura, N. Yoshida, K. Yamashita, Solid State Ionics **285**, 143 (2016)
5. R.D. Shannon, B.E. Taylor, T.E. Gier, H.Y. Chen, T. Berzins, Inorg. Chem. **17**, 958 (1978)
6. H.U. Beyeler, T. Himba, Solid State Commun. **27**, 641 (1978)
7. H.Y.-P. Hong, J.A. Kafalas, M. Bayard, Mater. Res. Bull. **13**, 757 (1978)
8. E. Banks, C.H. Kim, J. Electrochem. Soc. **132**, 2617 (1985)
9. K. Yamashita, M. Tanaka, T. Umegaki, Solid State Ionics **58**, 231 (1992)
10. K. Yamashita, T. Nojiri, T. Umegaki, T. Kanazawa, Solid State Ionics **35**, 299 (1989)
11. R.D. Shannon, T.E. Gier, C.M. Foris, J.A. Nelen, D.E. Appleman, Phys. Chem. Miner. **5**, 245 (1980)
12. F. Cervantes, L.J. Marr, F.P. Glasser, Ceram. Int. **7**, 43 (1981)
13. C.H. Kim, B. Qiu, E. Banks, J. Electrochem. Soc. **132**, 1340 (1985)
14. K. Yamashita, S. Ohkura, T. Umegaki, T. Kanazawa, Solid State Ionics **26**, 279 (1988)
15. T. Okura, M. Tanaka, G. Sudoh, Mater. Res. Soc. Symp. Proc. **453**, 611 (1997)
16. T. Okura, K. Yamashita, T. Umegaki, Phosphorus Res. Bull. **6**, 237 (1996)
17. T. Okura, M. Tanaka, H. Monma, K. Yamashita, G. Sudoh, J. Ceram. Soc. Jpn. **111**, 257 (2003)
18. K. Yamashita, T. Umegaki, M. Tanaka, T. Kakuta, T. Nojiri, J. Electrochem. Soc. **143**, 2180 (1996)
19. T. Okura, M. Tanaka, H. Kanzawa, G. Sudoh, Solid State Ionics **86–88**, 511 (1996)
20. K. Yamashita, M. Tanaka, T. Kakuta, M. Matsuda, T. Umegaki, J. Alloys Compd. **193**, 283 (1993)
21. K. Yamashita, T. Nojiri, T. Umegaki, T. Kanazawa, Solid State Ionics **40/41**, 48 (1990)
22. K. Yamashita, S. Ohkura, T. Umegaki, T. Kanazawa, J. Ceram. Soc. Jpn. **96**, 967 (1988)
23. W.D. Kingery, H.K. Bowen, D.R. Uhlmann, *Introduction to Ceramics*, 2nd edn. (Wiley, New York, 1976), p. 368
24. T. Okura, H. Monma, K. Yamashita, J. Ceram. Soc. Jpn. **112**, S685 (2004)
25. T. Okura, H. Monma, K. Yamashita, Solid State Ionics **172**, 561 (2004)
26. T. Okura, K. Yamashita, Solid State Ionics **136/137**, 1049 (2000)
27. T. Okura, Y. Inami, H. Monma, S. Nakamura, K. Yamashita, Solid State Ionics **154**, 361 (2002)
28. T. Okura, H. Monma, K. Yamashita, J. Eur. Ceram. Soc. **26**, 619 (2006)
29. S. Suda, K. Yamashita, T. Umegaki, Solid State Ionics **89**, 78 (1996)
30. T. Okura, H. Monma, K. Yamashita, J. Electroceram. **24**, 83 (2010)
31. I.W. Donald, J. Mater. Sci. **30**, 904 (1995)
32. Y.M. Sung, J. Mater. Sci. **31**, 5421 (1996)
33. H.U. Beyler, R.D. Shannon, Appl. Phys. Lett. **37**, 934 (1980)
34. I. Maki, T. Sugimura, J. Ceram. Soc. Jpn. **78**, 129 (1970)
35. P. Mondal, J.W. Jeffery, Acta Crystallogr. **B31**, 689 (1975)
36. M.G. Alexander, Solid State Ionics **22**, 257 (1987)
37. T. Okura, M. Saimaru, H. Monma, K. Yamashita, Solid State Ionics **180**, 537 (2009)
38. T. Okura, K. Kawada, N. Yoshida, H. Monma, K. Yamashita, Solid State Ionics **225**, 367 (2012)
39. I.W. Donald, J. Mater. Sci. **30**, 904 (1995)
40. Y.M. Sung, J. Mater. Sci. **31**, 5421 (1996)
41. T. Okura, T. Takahashi, H. Monma, K. Yamashita, Solid State Ionics **179**, 1291 (2008)
42. T. Okura, K. Kawada, N. Yoshida, H. Monma, K. Yamashita, Solid State Ionics **262**, 604 (2014)